THE ATOMIC MASSES OF ^{57}Cu AND ^{59}Zn

by

Bradley Marc Sherrill

A DISSERTATION

Submitted to
Michigan State University
in partial fulfillment of the requirements
for the degree of

DOCTOR OF PHILOSOPHY

Department of Physics and Astronomy

1985

To my wife

Carolyn Moravitz Sherrill

ACKNOWLEDGMENTS

I would like to thank the staff, students, and faculty of the NSCL for their support of my education. I recognize that without their contributions the following pages would not exist.

I wish to acknowledge those people, among others, who were instrumental in making the S320 a working device: W. Benenson, R. Blue, S. Bricker, M. Distasio, L. Harwood, E. Kashy, W. Lynch, J. Nolen, J. vanderPlicht, D. Swan, J. Winfield, J. Yurkon, and an army of undergraduates.

There are several people to whom I owe special thanks. J. Winfield, M. Lowe, and R. Fox have made significant contributions to SARA; for their suggestions and help I am greatly indebted. J. Nolen has been helpful in all aspects of my graduate work, in particular he has taught me a great deal about experimental equipment and techniques. B.A. Brown has also helped me a great deal. He not only supplied the computer codes to perform the calculations, but also is responsible for most of the theory presented in this thesis. Above all, the person most responsible for the completion of this thesis and my ability to do so is W. Benenson. His

support, encouragement and teaching were greatly appreciated.

I want to thank my parents Janice and Wesley Sherrill for helping me reach this point, and my grandparents Carl and Marie Mansheim and Florence Sherrill for the special role they have played in my life.

Finally, I want to thank the person who taught me the most important lessons of my graduate years, and gave me the necessary love and affection to make it through: my wife Carolyn.

I am also grateful to MSU and the National Science Foundation for financial support during my graduate study.

TABLE OF CONTENTS

LIST OF TABLES

LIST OF FIGURES

CHAPTER ONE

1.1 Motivation

The most fundamental property of any atom is its mass. From the mass the binding energy of the nucleus can be calculated, its decay modes predicted, and information on the nature of the nuclear force deduced. The abundances of the elements and their isotopes in the universe are due in large part to nuclear binding energies (C168,Ar79). Recently, based on atomic masses, predictions of new decay modes including proton decay (Fa84) and ^{14}C decay (Ro84a,St85a,Ga84) have been confirmed. Overall the importance of atomic masses can be understood when we note that indeed the mass of an atom is the lowest energy eigenvalue of the nuclear Hamiltonian.

Some of the first evidence for the shell model came from the change in slope of the binding energy curve for nuclei with magic numbers of neutrons and protons (Ma48,Ha49). In the present day, data on β-unstable nuclei still provide important information for shell model studies. Based on the properties of stable or near stable nuclei Wildenthal (Wi83) has developed a complete s-d shell

Hamiltonian. With this Hamiltonian, Wildenthal has predicted the halflives and masses of the neutron rich s-d shell nuclei. A test of the validity of the s-d shell Hamiltonian is to compare the predicted masses and lifetimes to the measured values for the s-d shell nuclei far from β-stability. This has been done for the nuclei with known properties, and in general the agreement is excellent, except for a region near ^{30}Na, where the mass excesses of very neutron rich Na isotopes are known (Th75,De83). This disagreement can be interpreted as a region of deformation. Further data on masses in the s-d shell will help understand the anomaly.

Mass data may indicate new degrees of freedom in other shells as well. In particular there are two regions where recent models have predicted new magic numbers. These are at ^{52}Ca (To81) and ^{146}Gd (Kl79). Currently, the masses of ^{51}Ca, ^{52}Ca and ^{147}Tb are unmeasured but are necessary for determining the validity of the predictions. In general new degrees of freedom are found by comparison of masses to predictions by the various models which predict atomic masses (for an almost complete summary see Maripuu (Ma76)).

Atomic mass models are based on assumptions ranging from the shell model to the liquid drop model. Some are also essentially empirical fits with thousands of free parameters. Since the mass is such a fundamental quantity, any global theory which could predict atomic masses must contain some fundamental information of the nuclear force.

Knowledge of, or the ability to predict atomic masses, is also essential to understanding the abundances of elements in the universe (Ar79). As a result there is great interest predictions of nuclear masses (see for example the proceedings of the Atomic Mass and Fundamental Constants conferences (AMCO), or the 4th International Conference on Nuclei far from Stability). Once a model has been developed, new masses far from β stability are needed to test the mass model validity. The farther from stability the model can predict, the greater its credibility.

Despite the great interest in atomic masses, of the 7000 isotopes which are predicted to be particle stable, only 1400 have known masses. The reason so few of the predicted particle stable isotopes have known masses is the difficulty in producing and studying nuclei far from β-stability. Only 284 isotopes are stable or have sufficiently long halflives that they are found naturally. In most cases the unknown isotopes must be synthesised from these nuclei. To date the largest deviation from the line of stability to measure a mass is 21 neutrons (Ro79), while β-stable nuclei are predicted up to a hundred neutrons away.

In this thesis the measurement of the mass of two nuclei far from β stability will be presented. As an indication of the importance of mass data, these results will be used to study the charge independence of the nuclear force, test a shell model for the f-p shell, and test previous assumptions used in astrophysical models involving

rapid hydrogen burning. Also as part of this thesis, techniques developed to perform mass measurements at the National Superconducting Cyclotron Laboratory at Michigan State University will be presented. Before beginning the discussion of these measurements, it is useful to review the techniques used to study nuclei far from β stability.

1.2 Introduction to Mass Measurements

The expression of mass which will be used in this thesis is the atomic mass excess defined as

$$ME = Mass - M_0 \times A \qquad (1.1)$$

where M_0= 931.5016 MeV is one atomic mass unit (AMU). The units used to quote mass will be MeV.

1.2.1 Stability Studies

There are many ways to determine the atomic mass excess of an exotic isotope. An upper limit on the mass excess can be determined by whether or not the isotope is particle stable. Historically, ^{14}Be, ^{11}Li, ^{19}C were predicted unstable, but were shown by experiment to be particle stable. Thus, the measurements which show the stability of an isotope are useful information for mass models.

Artukh et al. used deep inelastic transfer reactions with projectiles of ^{18}O (Ar69), ^{22}Ne (Ar70), and ^{40}Ar (Ar71a) to infer the stability of 28 new isotopes. They were also able to infer the instability of several isotopes

including ^{10}He (Ar71b). A review of the deep inelastic work was presented by Volkov (Vo78). Even earlier, proton spallation experiments were used to create nuclei far from β-stability (Po65,Bo74). More recently, proton spallation has been used in connection with an online mass separator to demonstrate the stability and measure masses and decay properties of very exotic K and Na isotopes (Th75,De83). Vieira has also used proton spallation and time-of-flight (TOF) techniques to identify and study neutron rich nuclei (Vi84). He and his colleagues plan to build a new, improved TOF spectrometer at LAMPF to measure the masses of nuclei produced in proton spallation reactions (Wo84).

Several groups have used high energy beams of ^{40}Ar (Sy79) and ^{48}Ca (We79,St81) from the Bevalac and the fragmentation mechanism to produce very neutron rich nuclei. Recently, Stevenson has demonstrated the particle stability of ^{19}B produced from the fragmentation of ^{48}Ca (St85b). Devices have now been built which will use the fragmentation mechanism to create nuclei far from β stability (Ha81b,Du84,La84). These devices can separate the reaction products by mass, which will allow decay properties and possibly masses to be studied for nuclei very far from β stability.

1.2.2 Decay Studies

Although useful in identifying new isotopes and in some cases studying decay properties, the above methods have not been generally useful in determining atomic mass excess.

The two general categories of experiments which have been used to determine atomic masses are decay studies and Q value measurements. Decay studies are usually performed on nuclei produced in fusion or fission reactions. Fusion reactions have been used at many laboratories, and the products separated by various types of devices such as online mass separators. Examples of this type of experiment are performed at GSI (Ro78) and CERN (Th75,De83). Fission studies are performed in such devices as COSIRIS (Bo71) and TRISTAN (Br80b).

The main technique by which many of the heavy elements, produced in either fusion or fission reactions, have had their mass excesses measured is by attempting to measure the maximum electron or positron energy from β decay, called β-endpoint measurements. The mass of an unknown isotope is derived from a known isotopes mass by

$$ME(unknown) = ME(known) + E_{\beta max} \qquad (1.2)$$

for β^- decay, and for β^+ decay

$$ME(unknown) = ME(known) + E_{\beta max} + 2m_e \qquad (1.3)$$

where m_e is the electron mass in MeV. If the decay is to an excited state in the daughter, then this excitation energy must also be known. Many authors have used this method. In fact, the Q value measurements presented in this thesis will

be compared to β-endpoint measurements for ^{57}Cu (Sh84a) and ^{59}Zn (Ar84). For examples of β-endpoint measurements and discussions of techniques, see any of the AMCO conference proceedings. The main problem in β-endpoint studies is that it is difficult to get good statistics near the endpoint. There is also usually background which must be subtracted from the spectrum. The response of the detector to the β energy is also an unknown and must be determined. The result is usually to limit the mass excess resolution to ±100keV or so. Since the nucleus being studied is also decaying, it is usually not possible to obtain information on the energy spectrum of that nucleus.

The other type of decay study, which yields a mass excess, is the study of α-chains ending in a known mass. In this case mass excess of very exotic nuclei can be inferred by

$$ME(\text{unknown}) = ME(\text{known}) + \sum_{\alpha} (ME(\alpha) + E_{\alpha}) \quad (1.4)$$

Again if any of the decays are to excited states the gamma ray energies must be measured and included. These types of studies have been performed on proton rich nuclei produced in fusion reactions (Ro78,Sc79, and Sc81 for example). The mass excesses which can be inferred have reasonable accuracy, but rely on a comparison to a single known mass. Also it is not always possible to connect α chains to known

masses. Finally, again no excited state information is obtained on the nucleus being studied.

One last method which can be used to measure atomic mass excesses from observing nuclear decays is to study the EC/β^+ ratio for proton rich nuclei (Ro84b). This ratio is sensitive to the mass difference between the mother and daughter. It is, in principle, reasonably accurate but is only applicable in a certain range of nuclei where this ratio is measureable. In general the β-decay energy for nuclei far from β-stability is large and the EC/β^+ ratio is extremely small, which makes it difficult to measure.

1.2.3 Q Value Measurements

The technique which has been used primarily in lighter nuclei to measure atomic mass excesses is the determination of the Q value of a reaction. The Q value is defined for the reaction A(B,C)D as

$$Q = ME(A) + ME(B) - ME(C) - ME(D) \qquad (1.5)$$

If the Q value can be measured and three of the involved masses are known, then the mass excess of the fourth can be determined. It is possible in fact to measure masses to better than 1 part in 10^7 with this method, which in the past have been more accurate than decay studies. The techniques and considerations for Q value measurements have been discussed by several authors (No74,Ka75,Th82). The

accuracy of this method relies on measuring the unknown Q value relative to known Q values.

It is possible to divide Q value measurements into two main categories. In the first type the nucleus to be studied is undetected. The mass excess of the particle D in the reaction A(B,C)D can be determined using two body relativistic kinematics and knowledge of the initial beam energy, scattering angle, and energy of the outgoing particle C. There have been many Q value measurements of this type, and it would be difficult to make a complete discussion of the work which has been done. Some examples of this type of measurement are the studies of mirror nuclei in the f7/2 shell by Mueller (Mu75) via the (^{3}He,^{6}He) and (^{3}He,^{7}Li) reactions. Benenson (Be79) has also used Q value measurements to study isobaric quartets in light nuclei. Some of the more exotic reactions studied of this type are the (π^{-},π^{+}) mass measurements of ^{14}Be (Gi84) and ^{18}C (Se78).

In the other general type of Q value measurement the nucleus to be studied is detected. An example of this method was the mass excess measurement of ^{17}C by the ^{48}Ca(^{18}O,^{17}C)^{49}Ti reaction (No77). This type of study is better in the sense that it is less sensitive to impurities in the beam or target, but it is more difficult to obtain excited state information on the nucleus of interest.

The main consideration for Q value studies, especially for studies on nuclei far from β stability, is the size of the cross section for the reaction. Since the cross section

drops as the reactions involve more nucleons and more complicated transfers and rearrangements, it is difficult to use Q value measurements to study nuclei very far from β stability. Although the reactions will involve the nuclear structure of the participants, it has been noted by several authors (An74,Po73,Br72) that in cases where the linear and angular momentum of the incoming and outgoing particles is matched, the reaction is favored. In general for reactions involving heavy ions this means high spin states in the residual nucleus will be favored because the angular momenta of the outgoing particle is much less than that of the incoming particle. However when the outgoing particle is heavier than the beam, it is possible to match momenta for the reaction if the appropriate beam energy is available. In these favorable cases the cross section for the reaction is expected to be a maximum for the ground state. Hence, in Q value measurements it is desirable to match, as close as possible, the momenta to maximize the cross section.

1.3 Thesis Material and Organization

In this thesis two exotic Q value measurements and their implications will be discussed. These reactions are $^{58}Ni(p,\pi^-)^{59}Zn$ and $^{58}Ni(^7Li,^8He)^{57}Cu$. With these reactions we were able to determine the mass excesses of ^{57}Cu and ^{59}Zn. These nuclei are interesting because they are $T_z = -1/2$ nuclei and are thus input for mass formula (Ke66) and provide data to study the Nolen-Schiffer anomaly (No69). Their β decays can also be used to investigate quenching of

Gamow-Teller strength in nuclear transitions. The nucleus ^{57}Cu is particularly interesting because it has, in a simple shell model, one proton outside the closed ^{56}Ni core. This makes its mass excess and level structure important for nuclear structure calculations and studies of the effect of the Coulomb force in nuclei. As we will see in chapter 5, the structure of ^{57}Cu is also important for nucleosynthesis, and in particular astrophysical models involving the rp-process (Wa81).

The organization of the thesis will treat the ^{57}Cu and ^{59}Zn measurements separately. Chapter 2 will describe the ^{57}Cu measurement, while chapter 3 will be devoted to the ^{59}Zn measurement. At the end of each chapter a discussion of the implications of the results for mass excess models and Gamow-Teller strengths will be presented. Chapter 4 will discuss the Nolen-Schiffer anomaly and the new data provided by these measurements. The possibility that this anomaly is evidence for charge symmetry breaking in the nuclear force will be reviewed. The rp-process will be discussed and its relation to the new ^{57}Cu data presented in chapter 5. The conclusions will be reviewed in chapter 6. The appendicies contain information on some of the experimental details related to the ^{57}Cu measurement. Appendix A discusses the magnetic optics calculations done for the design of the S320 spectrometer used in the ^{57}Cu mass measurement. Appendix B is a description of an octupole magnet which was designed and constructed to

improve the resolution of the spectrograph. Finally, appendix C is a description of the data taking program, SARA, used in experiments on the S320 spectrograph.

CHAPTER TWO

2.1 Introduction

The first atomic mass measured at the National Superconducting Cyclotron Laboratory (NSCL) with the K500 cyclotron was that of ^{57}Cu. The measurement was performed by determining the Q value of the ^{58}Ni(^{7}Li,^{8}He)^{57}Cu reaction, as part of this thesis. This reaction was chosen for the first attempt because of several advantages; thick targets could be used, ^{8}He has no excited states, and the cross sections were expected to be large since at the K500 beam energies it is possible to match the incoming and outgoing angular momenta of the ^{7}Li and ^{8}He nuclei. To match the incoming and outgoing particles angular momenta in the ^{58}Ni(^{7}Li,^{8}He)^{57}Cu reaction, as was discussed in the introduction, one needs a ^{7}Li beam energy of ~175MeV. The ^{8}He energy after the reaction is ~150MeV. To bend a ^{8}He nucleus with that energy requires a spectrograph with a K parameter of 280, where $K=(MeV/u)(u/q)^2$. Very few spectrometers with such a large K exist anywhere in the world. The HRS at Los Alamos (En70), GSI's simple

spectrograph (Sc83), and Big Karl (Ma83) at the KBI are examples. However, the NSCL is unique in the combination of the correct ^{7}Li beam energy and a K=320 spectrograph. Thus, the ^{58}Ni(^{7}Li,^{8}He) Q value measurement was proposed and performed at the NSCL.

The nucleus ^{57}Cu has received much attention, because it is a simple nucleus with one proton outside a ^{56}Ni closed core. It has only been observed twice, and most of its properties are not well known. It was observed first in a study of β-delayed proton emission from ^{57}Zn (Vi76). Because of the nature of the experiment only high excitation proton unbound states were observed. The other observation was reported in a preliminary report from a group at Tohoku University(Sh84a,Mi83), where ^{57}Cu was produced via the ^{58}Ni(p,2n) reaction. They measured the ^{57}Cu lifetime to be 233±16 msec and Q_{β}=7.72±0.13 MeV. Because ^{57}Cu has one proton outside the ^{56}Ni closed core, it makes data on the low-lying states and mass of ^{57}Cu very useful for studying nuclear structure effects in the fp shell, and in particular studying the effects of the Coulomb force in nuclei. One particular application of this data is in studying the Nolen-Schiffer anomaly(No69). Further, due to the role closed core nuclei play in nature, ^{57}Cu is important for astrophysical models. The primary model for which data on ^{57}Cu is needed is the rp-process(Wa81,Wa83). However, ^{57}Cu is difficult to study because it is 6 neutrons lighter than the first β-stable Cu isotope, ^{63}Cu. This means production

cross sections for transfer reactions are low and the lifetime is short.

In this chapter the experimental setup of the S320 spectrograph will be discussed, including the magnetic layout, detector, electronics, and the data acquisition system hardware and software. The mass measurement results, information on cross sections for the (^{7}Li,^{8}He) reaction, and level structure will be presented. The measured mass excess will be compared to standard nuclear mass models and the extracted Gamow-Teller (G-T) matrix elements compared to those calculated by the shell model. For a case such as ^{57}Cu one would expect the shell model calculations to be very good if the ^{56}Ni core is indeed doubly magic. The closed core nature of ^{56}Ni also makes the nucleus ^{57}Cu a particularly good case to study the Nolen-Schiffer anomaly because corrections to the calculated Coulomb displacement energy which depend on nuclear structure should be calculable. The Nolen-Schiffer anomaly will be discussed in chapter 4. The new information obtained on ^{57}Cu may also significantly influence the rates of element production for A>56 from the rp-process and the energy generation at late times in such a process. This will be discussed in detail in chapter 5.

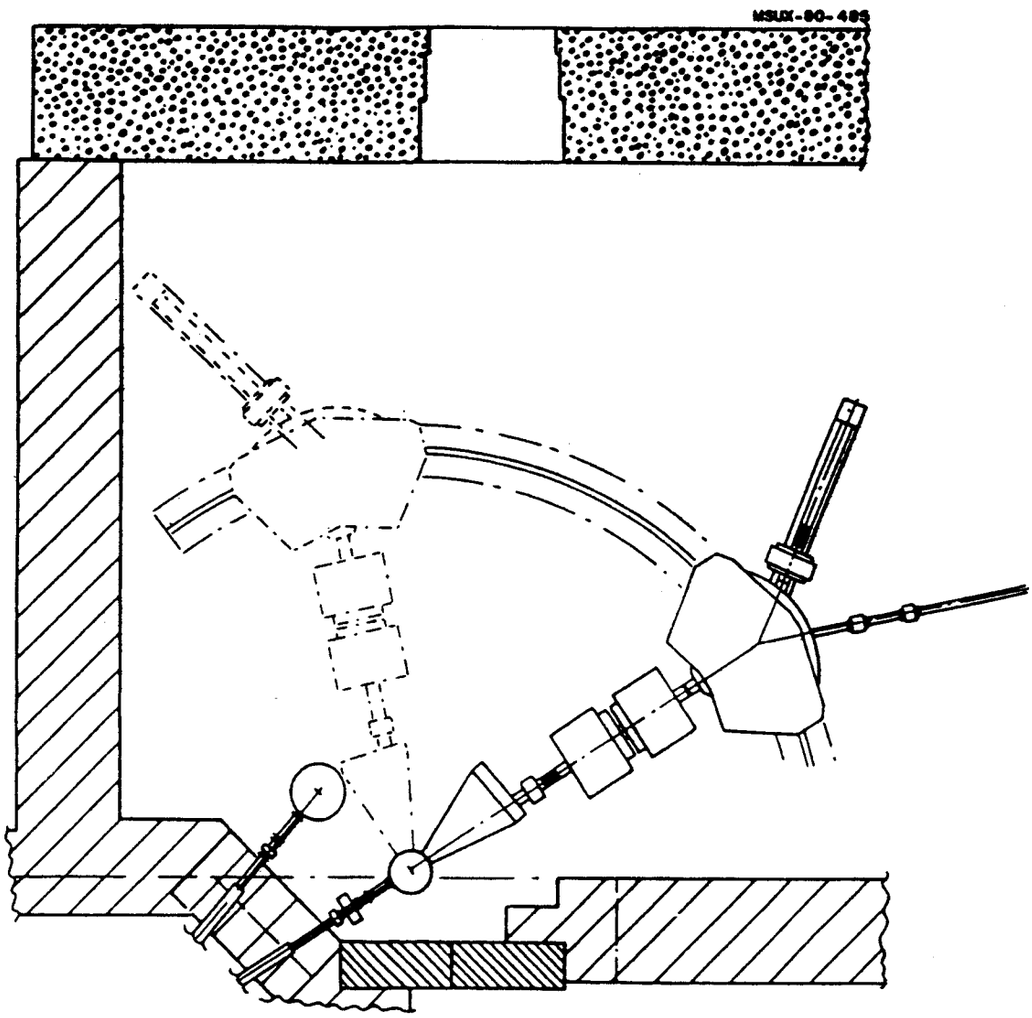

Figure 2-1: Top view of the S320 spectrograph.

Table 2-1: Parameters for the S320 Spectrograph.

Dispersion:	1.6 cm/% ($\Delta p/p$)
Magnification:	$M_x = -0.67$ (D/M=2.4)
	$M_y = -2.5$
Assumed target spot size:	0.5mm incoherent width
	3mm tall, dispersion
	matched (2.5cm/% opt.)
Solid Angle:	$\Delta\theta = \pm$ 12mr
	$\Delta\phi = \pm$ 12mr
	Ω = 0.56 msr
Calculated Line Width:	$\Delta E/E \leq 0.1\%$, 0.8mm
Range:	$\Delta E/E$ = 20%
	60 MeV at 300 MeV
Focal Plane:	Normal incidence,
	16cm long by 2.6cm tall
Maximum Rigidity:	$B\rho_{max} = 2.57$ T-m at
	B = 1.47 T
	$\rho_{max} = 1.75$ m

1.2 Experimental

1.2.1 The S320 Spectrograph

The measurements were performed in the K=320, S320 spectrograph. A top view of the spectrograph is shown in Figure 2-1. A schematic view of the component layout and beam envelopes calculated with the program TRANSPORT(Br77b) are shown in Figure A-3. The details of the S320 optical design will be presented in appendix A. The important optical and magnetic parameters for the S320 spectrograph are given in Table 2-1. The spectrograph is operated in the dispersion-matched mode with kinematic effects corrected by retuning the quadrupole doublet, as described in appendix A. The energy range of the device, 20%, or 60MeV at 300MeV beam energy, is adequate, but the small solid angle, 0.5msr (QDDD spectrometers have typically 14msr solid angles), makes collection times for experiments longer, and makes some low cross section experiments unfeasible. Due to the low solid angle, the minimum cross section which can be measured in a 3 day run, given typical K500 intensities, is 10 nb/sr. The 0.1% design energy resolution has not been reached to date. This may be due to a beam energy spread larger than the expected 0.1%, or an incoherent spot size larger than the assumed 0.5 mm. A detailed study to determine the cause of the failure to reach the design resolution has not been performed. The best energy resolution achieved thus far is 0.15%. In the present experiment, the thick targets used limited the resolution to values greater than 0.2%.

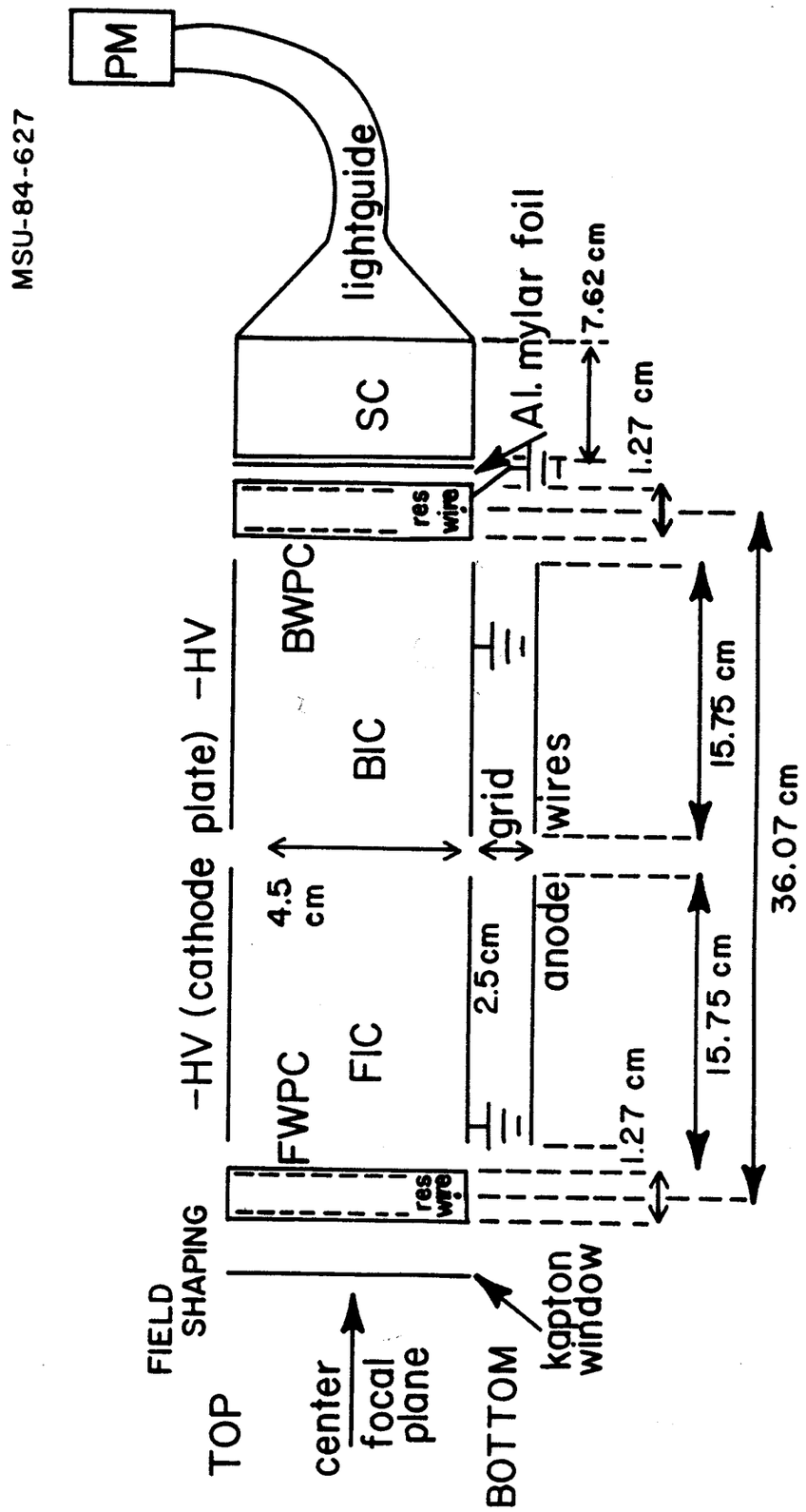

Figure 2-2: Schematic view of the S320 detector.

1.2.2 The S320 Detector

A schematic side view of the S320 detector is shown in Figure 2-2. The detector consists of two position sensitive proportional wires separated by ~40cm, and two ion chambers for energy loss information. The detector is backed with a 7.62cm thick plastic scintillator used for an event trigger, light output information, and a start signal for time-of-flight (TOF) against a stop from the cyclotron RF. This time provides a signal which is dependent on the particle velocity in the spectrograph. This detector has been described elsewhere in more detail by Yurkon et al.(Yu82).

2.2.3 Electronics

The electronics used for this experiment were relatively simple and are shown in the schematic diagram of Figure 2-3. There were nine signals which were recorded from the detector and processed by the electronics. An event was defined as a scintillator anode pulse above a CFD discriminator level set to gate out room background. The left and right signals from each wire were digitized, and the position was calculated by computer. The difference in position between the front and back wires was taken as a measure of the scattering angle relative to the central angle of the spectrograph. This is true because in first order $\theta_f = (\theta/\theta) \times \theta_i$, where $\theta_{i(f)}$ is the initial (final) scattering angle relative to the central spectrograph angle; higher order corrections are small. The anode signals were read from each ion chamber.

MSU-84-615

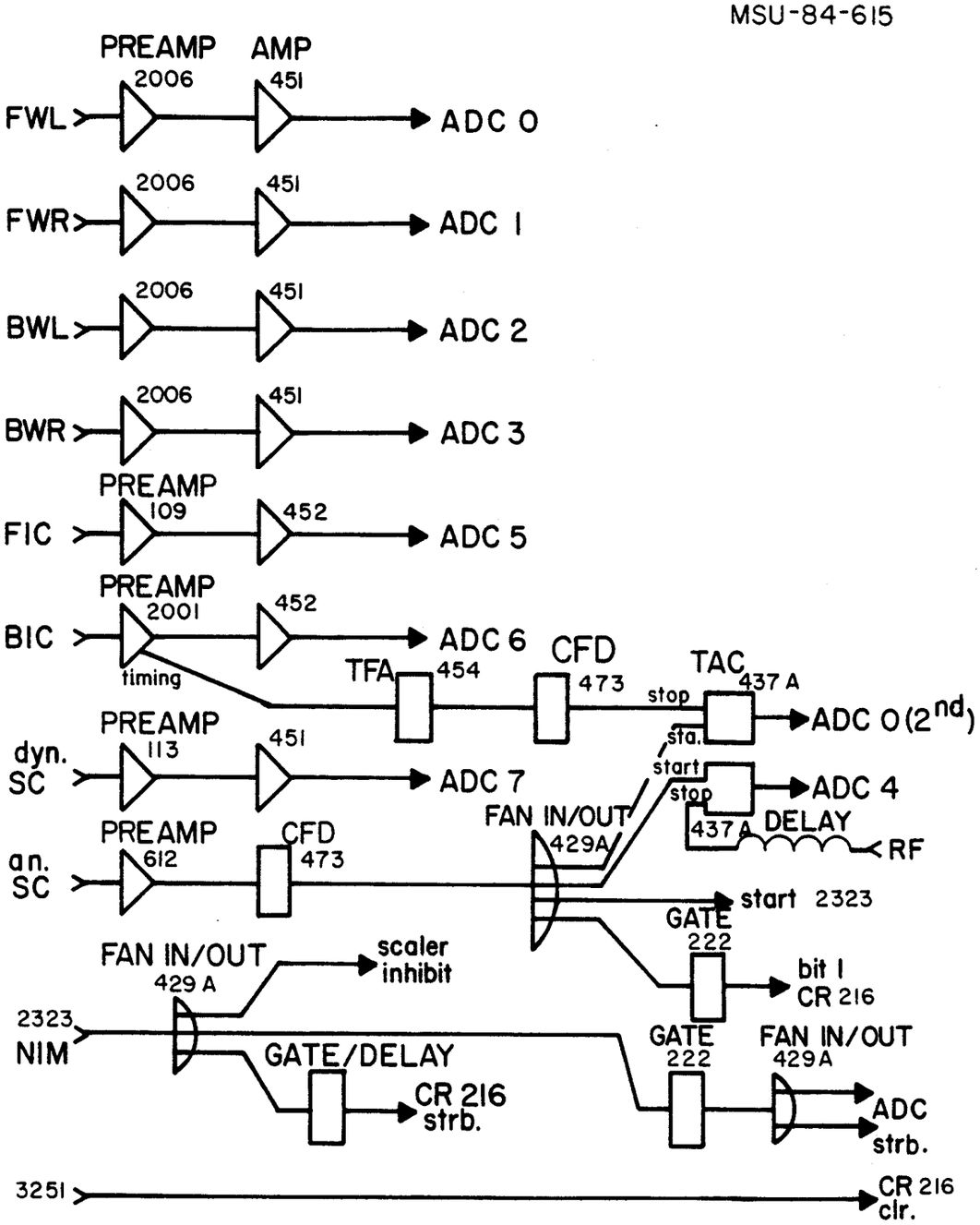

Figure 2-3: Schematic view of the S320 electronics.

A light output from the scintillator was read via the dynode signal from the scintillator phototube. Finally, two times were recorded using TACs. The drift time of the ions in the second ion chamber relative to the start pulse from the scintillator was used for y-height information. Also, the difference in time between a start from the scintillator and the next cyclotron RF pulse was recorded to measure velocity.

The signals were digitized with an ORTEC AD811 12bit ADC. The ADCs were read by an LSI-11 microcomputer acting as a smart CAMAC crate controller. The CAMAC data acquisition has been described in detail by Au et al. (Au83). The code to run the LSI was generated by the code SPECTRO written by R. Fox and D. Notmann(Fo84). The LSI stored events until an 8192 byte buffer was full, at which time the data was passed via a Kinetic Systems dataway interface to a VAX 11/750 computer. In the VAX an acquisition program named ROUTER distributed the data to subtasks which recorded the data on tape, recorded scalers, binned data, etc. The data display and analysis part of this system along with some details of the ROUTER system are discussed in appendix C. The online data acquisition system allowed the data to be monitored and analyzed as it was taken. In the case of the ^{58}Ni(^{7}Li,^{8}He) experiment it was almost possible to analyze the ^{8}He spectrum as it was taken. The same acquisition system was used offline to reread the data back from tape to perform more detailed analysis.

2.2.4 Particle Identification

The particle ID spectrum obtained for the $^{58}Ni(^{7}Li,^{8}He)^{57}Cu$ reaction is shown in Figure 2-4. The data are summed over angles ranging from 4 to 7 degrees. The detector gas was isobutane at a pressure of 70 Torr. Plotted in the figure is TOF vs. ΔE in the ion chamber and LIGHT output. In the TOF-ΔE spectrum the $^{8}HE^{2+}$ ions overlap with the $^{4}He^{1+}$ ions since both have the same velocity ($\Delta E \propto (Z^2/v^2)$ and $TOF \propto v$). However, the light output which is approximately proportional to $E^{1.7}$(Be74) separates the two because the $^{8}He^{2+}$ ions will have three times the $^{4}He^{1+}$ ions light output. Requiring counts to fall in the proper region of both plots clearly identifies the $^{8}He^{2+}$ ions. The TOF-LIGHT plot has some background, which may be due to the plastic's sensitivity to neutrons.

Two other particle groups which are prominent in the particle ID spectra are tritons and $^{7}Li^{2+}$ elastic scattering. The tritons, which are probably from some process such as a 3-body reaction, dominated the detector count rate at 1000 tritons/sec for a 20pnA beam. In contrast, the $^{8}He(^{57}Cu$ g.s.) rate was 0.5/hr. The triton energy spectrum for a typical run with θ_{sp}= 5 degrees and B_{sp}= 14.289 kG is shown in Figure 2-5.

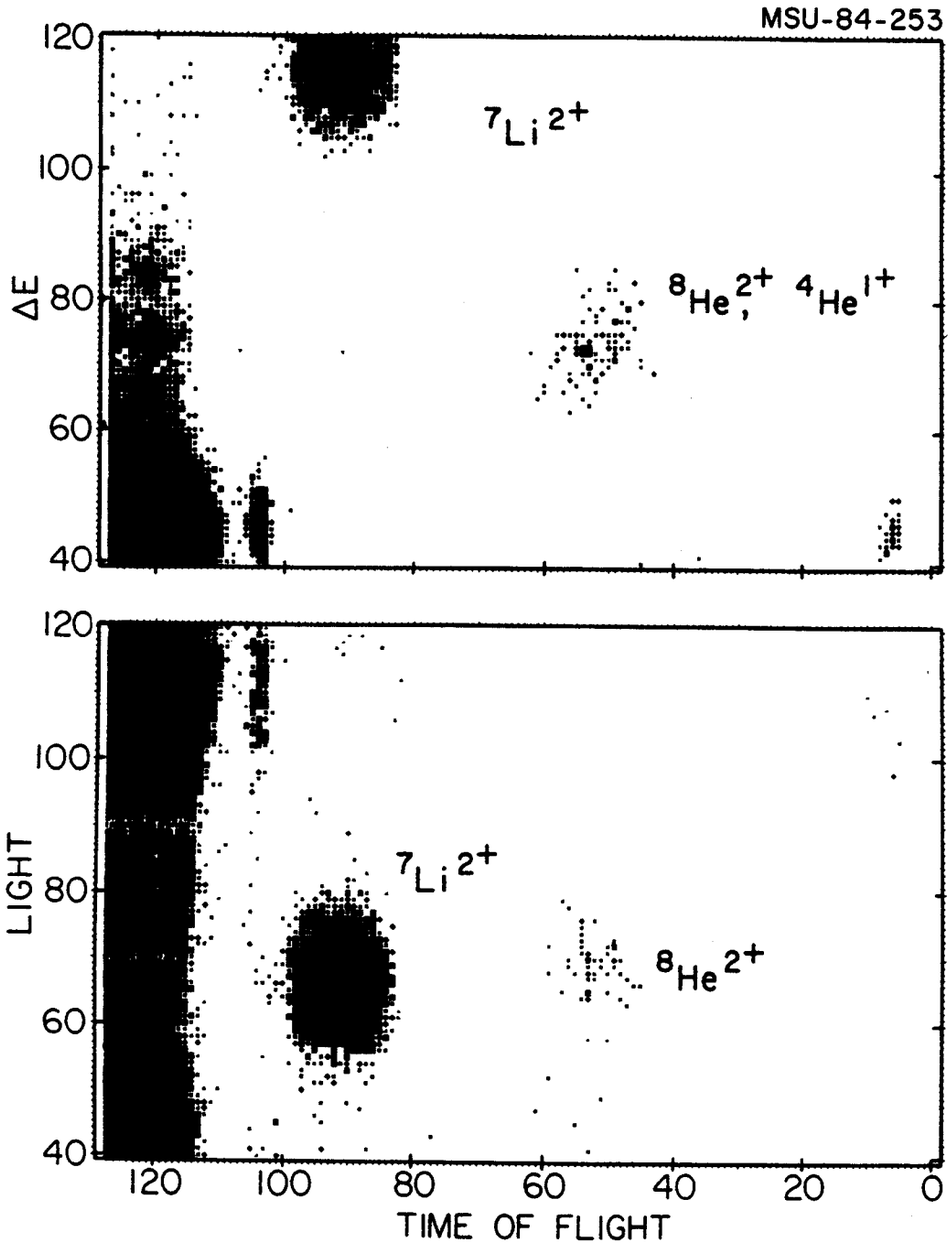

Figure 2-4: Particle ID for the $^{58}Ni(^{7}Li,^{8}He)$ reaction.

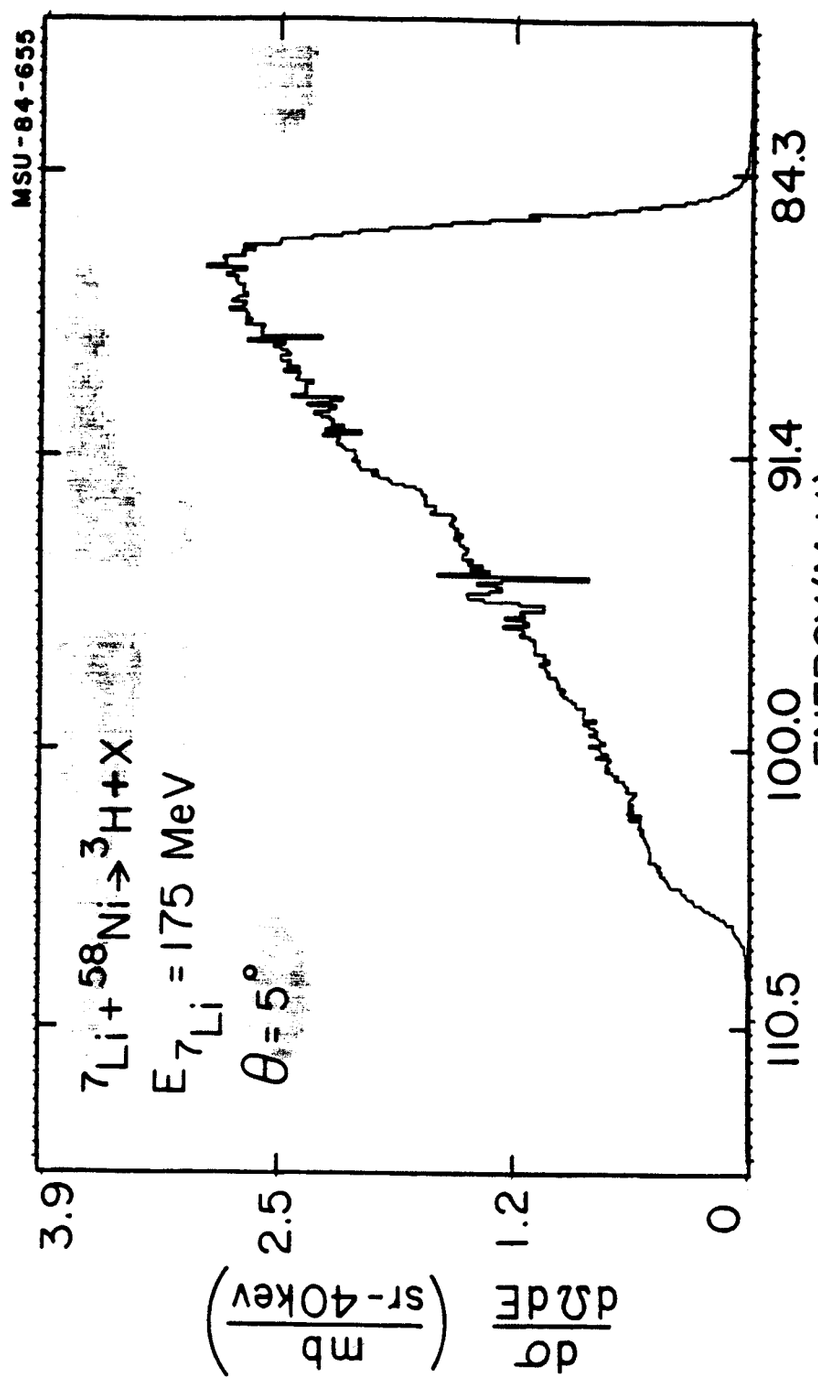

Figure 2-5: Triton energy spectrum for a typical run.

The apparent structure near E=107 MeV is due to roundoff errors in the position calculation since the triton energy loss in the proportional wires is very low and the signals were small. It might be interesting to investigate the mechanism which creates such large cross sections for tritons with velocities well above the beam velocity.

As seen in the particle ID spectra, the $^{7}Li^{+2}$ elastic peak also falls in the detector. We found the ratio between $^{7}Li^{2+}$ and $^{7}Li^{3+}$ at E_B= 175. MeV to be 9×10^{-5}. The elastic peak allowed the stability of the beam analysis system, cyclotron, and spectrograph to be monitored over the 3 days of the experiment. During long runs at constant dipole magnetic field, shifts of the order of 30 keV were observed. No evidence was seen for significant ^{12}C build up on the target, which would appear as a constant shift of the elastic peak.

2.2.5 Targets

The targets used were a 3.81(7) mg/cm^2 ^{58}Ni (99.93% enriched) target and a 3.03(6) mg/cm^2 ^{27}Al calibration target. The target thicknesses were determined by taking the weighted average of thicknesses determined by weighing and determined by the energy loss of α particles from a standard ^{241}Am α source. The α source measurement also showed that the targets were uniform to ±0.04 mg/cm^2 over the region of the targets used in the experiment. To accurately determine the energy loss of the ^{7}Li and ^{8}He nuclei in the target material, it is not only necessary to

know the target thicknesses but also the stopping power of the target material. The standard technique is to obtain the stopping powers from tabulated values (Ho80,Zi80). To test the validity of the tabulated values for our energies and ions, we measured the relative energy loss between a 3.81(7) mg/cm^2 ^{58}Ni target and a 2.10(5) mg/cm^2 ^{58}Ni target for 173.4 MeV ^{7}Li and 145.0 MeV ^{6}He ions. Using the relative energy loss, we measured stopping powers of 0.140 MeV/mg/cm^2 for the ^{7}Li ions, and 0.062 MeV/mg/cm^2 for the ^{6}He ions. The tabulated values of Ziegler are 0.135 MeV/mg/cm^2 for the ^{7}Li ions and 0.051 MeV/mg/cm^2 for the ^{6}He ions. In extracting the experimental stopping powers a linear dependence on energy was assumed and the stopping powers quoted are for the average energy of the ion in the target. Due to the agreement, the tables of Ziegler were used in determining all target energy losses for this experiment.

1.2.6 Calibration

A critical ingredient in any mass measurement is the spectrograph focal plane calibration. The accuracy of the calibration will limit the accuracy of the mass determination. Depending on the experiment the absolute beam energy may also be a critical factor. In this experiment a 200 keV uncertainty in the beam energy (out of a total beam energy of 175 MeV) meant a 24 keV uncertainty in the mass. However this uncertainty could be larger if the calibration particle and the measurement particle have

significantly different energies with similar magnetic rigidities. In this experiment the functional dependence of position in the focal plane with energy is determined with $^{7}Li^{+2}$ elastic scattering by varying all magnetic fields in the spectrograph by a given percent change and recording the change in position. The absolute Q value scale is set by measuring a reaction with a known Q value, in this case $^{27}Al(^{7}Li,^{8}He)^{26}Si$. The beam energy is also determined with the ^{27}Al target by measuring the difference between the ^{26}Si g.s. and the $^{7}Li^{+2}$ elastic peak which is sensitive to the beam energy. The calibration can be checked by measuring a reaction with known excited states. In this case the calibration was checked by taking a spectrum from the reaction $^{58}Ni(^{7}Li,^{6}He)^{59}Cu$. The spectrum is shown in Figure 2-6. The measured energy levels are compared to known levels from an equivalent (^{3}He,d) reaction(Bi76). The comparison is shown in Table 2-2. The rms deviation of the known states to the measured ones is < 20 keV, which is adequate for this experiment. The measured mass excess for ^{59}Cu is also only ~20 keV from the expected value. This agreement in the measured mass excess is better than expected because it was necessary to lower the dipole magnetic field by ~1 kG to study the ($^{7}Li,^{6}He$) reaction. This usually introduces field scaling errors which would not be included in the calibration.

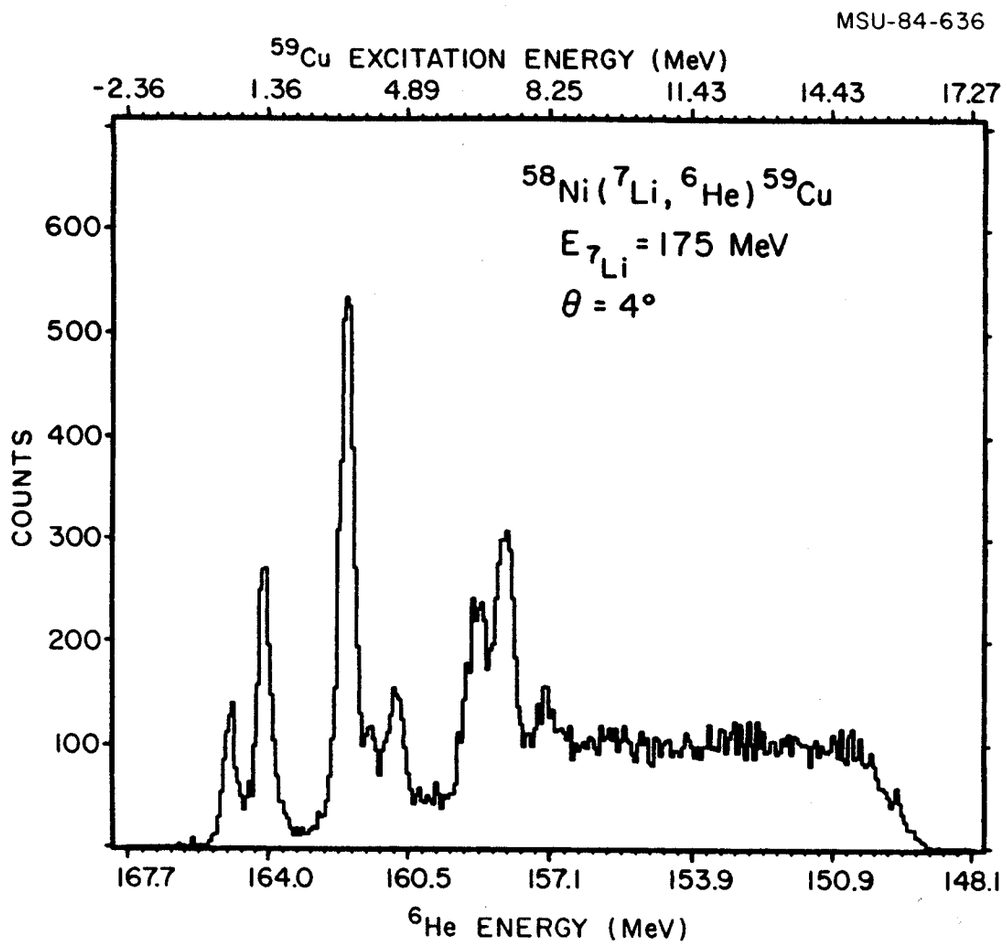

Figure 2-6: $^{58}Ni(^{7}Li,^{6}He)$ spectrum used as a check of the S320 focal plane calibration.

Table 2-2: Calibration comparison of levels measured with the $^{58}Ni(^{7}Li,^{6}He)$ reaction to those known from the $^{58}Ni(^{3}He,d)$ reaction.

B = 13.363 kG, θ = 4.0 deg:

$^{58}Ni(^{7}Li,^{6}He)^{59}Cu$	$^{58}Ni(^{3}He,d)^{59}Cu$ (Bi76)
0.0 MeV	0.0 MeV
0.896	0.913
3.031	3.047
4.330	4.307
6.203	6.202
6.945	6.937

The calibration calculations were carried out with the program CALIB. The general method is for the program to read an input file of calibration points, in this case elastic scattering, and to perform a polynomial fit of position in the focal plane, x, versus magnetic bend radius, ρ. A particle of given momentum, p, and charge q, will have a unique magnetic rigidity, Bρ. Hence given B, p, and q; ρ can be calculated and fitted versus x, which is measured. Once the fit has been performed, given any other x, ρ can then be determined. Then given B and q, the momentum and hence the energy of the particle can be determined. Using these techniques the program CALIB performs several options, including calculating the expected position for an ion from a given input reaction, excitation energy for a given channel number and reaction, and particle energy from a given channel number.

2.3 Results

The spectra obtained from the ^{58}Ni(^{7}Li,^{8}He)^{57}Cu reaction and the ^{27}Al(^{7}Li,^{8}He)^{26}Si calibration reaction are shown in Figure 2-7. The ^{57}Cu data is integrated over the angular range of 4 to 7 degrees, while the ^{26}Si data is from 5 degrees. The absence of counts below the lowest observed state in ^{57}Cu indicates good ^{8}He particle identification and a high purity ^{58}Ni target. Assuming the state at lowest excitation energy is the ^{57}Cu ground state, we measure a Q value of -29.564(54) MeV, which leads to a mass excess of ^{57}Cu of -47.35(5) MeV.

MSU-84-254

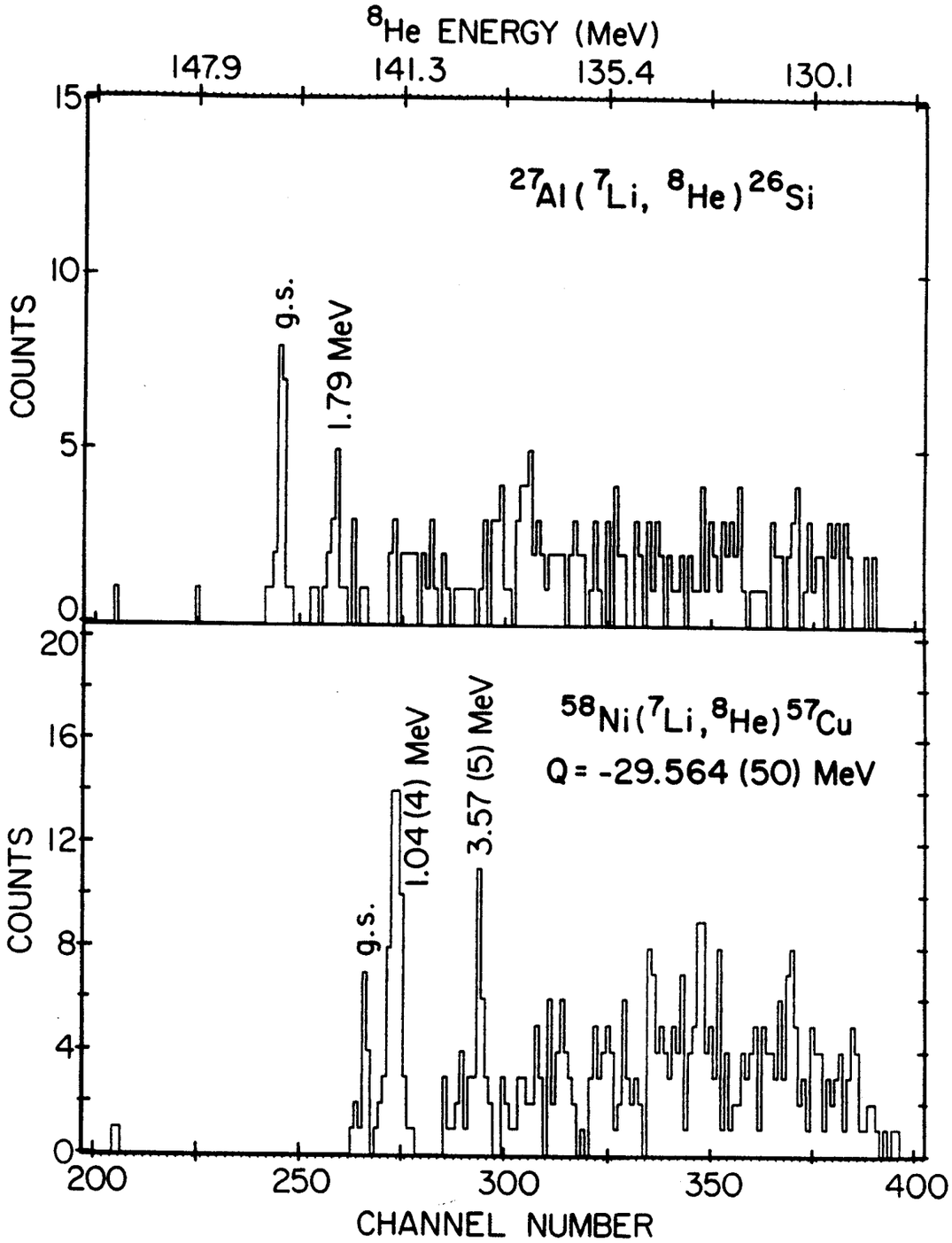

Figure 2-7: Position spectra for ^{8}He particles.

Table 2-3: Sources of uncertainty in the ^{57}Cu mass excess.

Parameter	Uncertainty in parameter	Mass Resolution (keV)
Target Thickness	2%	13.
Uniformity	1%	4.
Beam Energy	200 keV	24.
Angle	0.1 deg	9.
Statistics	^{26}Si g.s.	23.
	^{57}Cu g.s.	33.
Calibration		20.
		TOTAL 54.

(contributions added in quadrature)

The contributions to the uncertainty in the measurement are shown in Table 2-3. The primary uncertainty is from statistical uncertainties in the ^{26}Si g.s. and the ^{57}Cu g.s. centroids. These uncertainties added quadrature give 40 keV. The other two major sources of error are; 24 keV from uncertainty in the beam energy, and 20 keV from the uncertainty in the focal plane calibration. To obtain the final total uncertainty all effects were added in quadrature.

Figure 2-8 shows the measured levels of ^{57}Cu relative to its mirror nucleus, ^{57}Ni. The $1/2^-$ and the $5/2^-$ states are expected to lie within 50 keV of each other according to calculations of the displacement energies of these states and the structure of the mirror nucleus. The calculation is equivalent to treating the Coulomb force in first order perturbation theory and using the ^{57}Ni wave functions and energy levels as the unperturbed values. The calculations of the displacement energies reproduce quite well the trends in nearby nuclei and will be discussed in chapter 4 in connection with the Nolen-Schiffer anomaly. A statistical analysis of the peak at 1.04 MeV shows that its width is identical to that expected from the spectrograph resolution and the finite target thickness. However, a strong selectivity of the (^{7}Li,^{8}He) reaction for one of these states and not the other is not expected because the states are both single particle in composition.

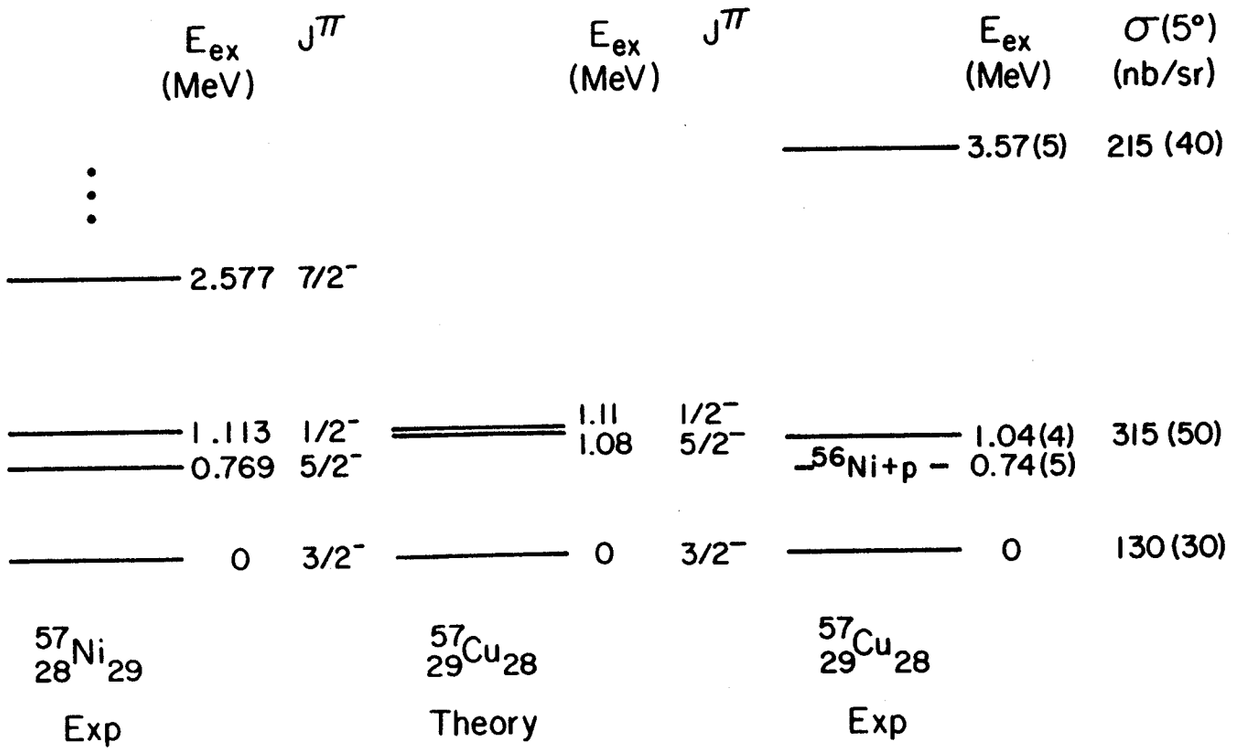

Figure 2-8: The level structure of ^{57}Cu along with the predicted structure based on pertubation theory and the structure of ^{57}Ni, mirror nucleus of ^{57}Cu.

Also, since the angular momentum mismatch between the incoming and outgoing particles is approximately 1.4 h, there should not be the selection of high spin states which is usually seen in heavy-ion reactions(Br72). Therefore we believe the $1/2^-$ and $5/2^-$ states both lie near 1.04(4) MeV excitation. It is possible, however, that only one of the states is populated, in which case the excitation of the other would be unknown. The quoted error of 40 keV for these states is included due to the uncertainty associated with the overlap of these states.

The limited angular distributions obtained for the measured states are shown in Figure 2-9. The error bars on the points reflect only the statistical uncertainties, $\sqrt{N}$, where N is the number of counts. Any systematic errors would shift the overall scale. No change in relative excitation is seen as a function of angle. In an attempt to understand the reaction mechanism two types of DWBA calculations were performed. First, since the low-lying states in ^{57}Cu are expected to be single particle states outside a ^{56}Ni core, one might hope to reproduce the results with DWBA calculations for the ^{56}Ni(^{9}Li,^{8}He)^{57}Cu reaction on the assumption that the l-transfer in this process will dominate the contributions from both the first step of this assumed route, ^{58}Ni(^{7}Li,^{9}Li)^{56}Ni, and all of the other possible reaction channels. These calculations were performed with the code SATURN-MARS (Ta74).

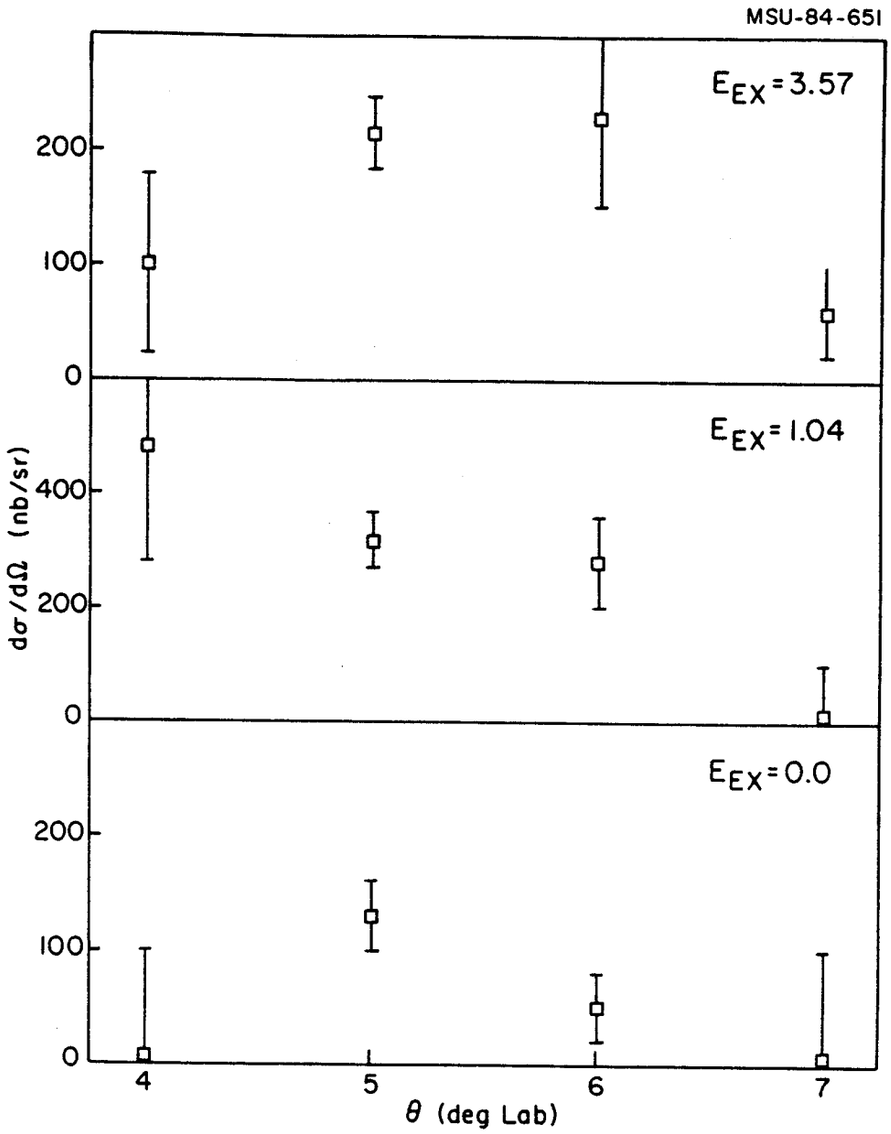

Figure 2-9: Angular distributions for the measured states in ^{57}Cu.

However, the predicted angular distributions did not match the data. In an attempt to determine if the reaction is more complicated, a sample two-step calculation assuming the simplest case of an l=0 two neutron pickup as the first step and the one proton stripping reaction as the second step, with the ground state of ^{56}Ni as the intermediate stage, were performed with the code SESIME (Pr76). Neither the relative magnitude of the cross sections for the observed levels or the angular distributions were reproduced. We conclude that the complexity of the (^{7}Li,^{8}He) rearrangement reaction, which is equivalent in quantum numbers to a Δ^{-} transfer from target to beam, makes it difficult to interpret in any simple way. We believe further study of the mechanism of the (^{7}Li,^{8}He) reaction would be interesting.

2.4 Comparison with Mass Models

2.4.1 Comparison

It is interesting to compare the measured mass excess to those predicted by the standard models. This comparison is shown in Figure 2-10. The predictions are taken from (Ma76). The error bars on the theoretical points represent the RMS deviation of the models with all known masses. The width of the line represents the uncertainty in this measurement.

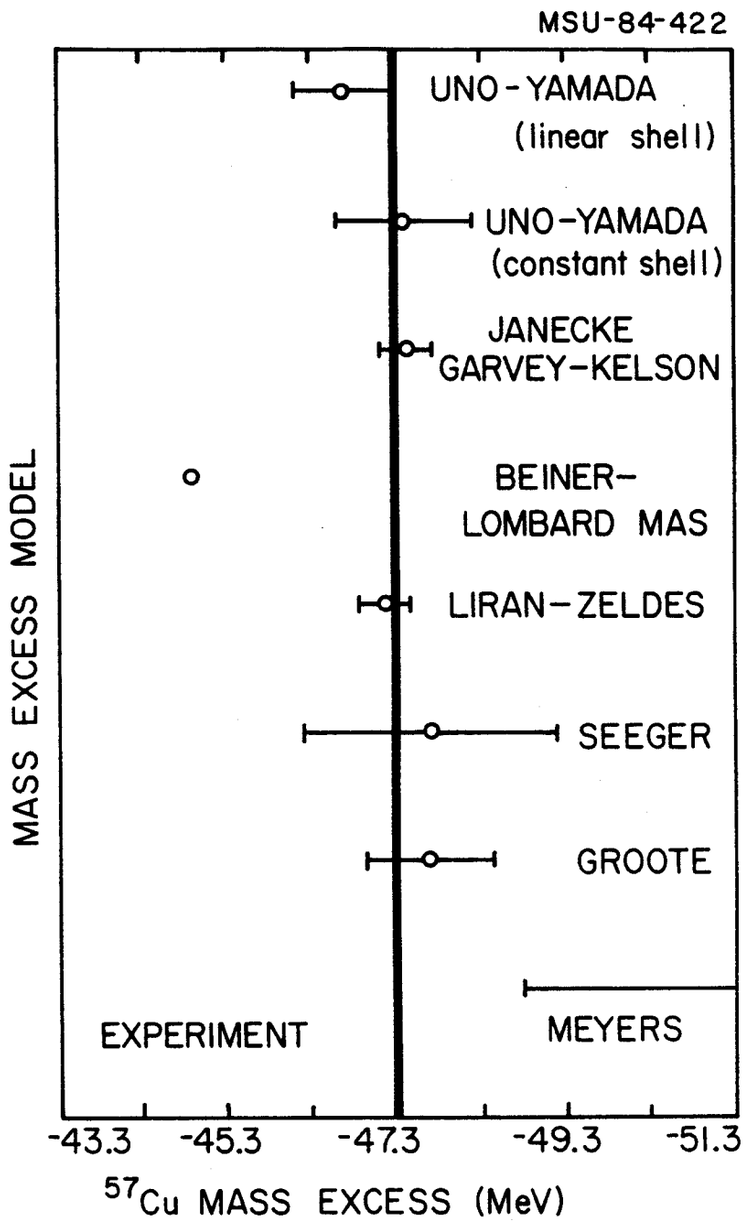

Figure 2-10: Comparison of the ^{57}Cu mass excess to various mass models.

The agreement indicates that the degrees of freedom in the models are sufficient to predict the ^{57}Cu mass excess. For a review of the various models see Maripuu (Ma76). Our measured mass excess also agrees with the β-endpoint measurement of Miyatake and Shinozuka (Mi83,Sh84a) of -47.36(13) MeV but has much better accuracy.

2.4.2 Garvey-Kelson Predictions

The mass excess of ^{57}Cu is also input into the Garvey-Kelson charge symmetric mass relation (Ke66). This mass relation is derived from the apparent charge independence of the nuclear force (charge independence will be discussed in detail in chapter 4). Hence the mass difference between analogue nuclei, $M(A,T=-T_z)$ and $M(A,T=T_z)$, is given by the Coulomb interaction. These Coulomb energies could be estimated from theoretical or phenomenological considerations or from a combination of each (see Ja68, or Chapter 4). Garvey and Kelson introduced a technique for evaluating the Coulomb energy and hence a method to predict the masses of proton rich nuclei provided the analogue neutron rich nucleus was known. The technique assumes a single particle model and determines the Coulomb energy for a proton in a given orbit by the difference between the mass excess of mirror nuclei with a valence particle in that orbit. Thus we write the the mass difference between analogue nuclei as

$$M(A,T_z=-T) - M(A,T_z=T) \approx \sum_{A'} [\, M(A',-1/2) - M(A',+1/2) \,] \quad (2.1)$$

where the sum runs over A' from A-(2T-1) to A+(2T-1) in steps of two. With this relation reliable predictions, with estimated errors of less than 100 keV, can be made for proton rich nuclei with N<Z (Ja68). Using the new data for ^{57}Cu, the mass excess predictions for lighter Cu isotopes are listed in Table 2-4. As shown in the table, ^{57}Cu is close to the predicted proton drip line.

2.5 Gamow-Teller Matrix Elements

2.5.1 Introduction

One interesting question which this new data may help answer is the goodness of the ^{56}Ni core. From the excitation spectra of ^{57}Ni it appears the energy gap between the f7/2 and 2p3/2 orbits is around 2.5 MeV. Thus, one might expect some admixture of the core in ^{57}Cu, but overall that ^{57}Cu is single particle in nature. A test is to use the known lifetime of ^{57}Cu and its mass excess to extract the ft-value for beta decay and hence the Gamow-Teller (G-T) matrix elements. These can be compared to those calculated in an extreme single particle model. Agreement would indicate a closed ^{56}Ni core. It must be noted however that exact agreement is not expected. Brown and Wildenthal have observed a quenching factor of 0.78 in s-d shell $\langle\sigma\tau\rangle$ values (Br83b).

Table 2-4: Garvey-Kelson charge symmetric mass predictions for Cu isotopes. Also shown are the one and two proton separation energies for these nuclei.

A	N	Z	Mass Excess	1 Proton Sep.	2 Proton Sep.
57	28	29	-47.35(5)	0.74	7.902
56	27	29	-38.614	0.574	5.183
55	26	29	-31.750	-0.176	3.688
54	25	29	-21.805	-0.316	2.083
53	24	29	-13.817	-1.570	0.975

The mechanisms for this quenching were studied by Brown and Wildenthal and also recently have been reviewed by Towner and Kahana (To83). We expect a similar quenching in the f-p shell.

2.5.2 Extraction of Measured Values

The G-T matrix elements can be extracted from experimentally measured lifetimes, branching ratios, and mass excess. This is true because the partial halflife for the β decay between an initial state $|i\rangle$ and a final state $|f\rangle$ is given by (see for example (Sh74))

$$t_{1/2} = C[(f_V + f_{EC})\langle\tau\rangle^2 + (f_A + f_{EC})(G_a/G_v)\langle\sigma\tau\rangle^2]^{-1}, \quad (2.2)$$

where $\langle\tau\rangle^2$ is the Fermi matrix and $\langle\sigma\tau\rangle^2$ is the Gamow-Teller matrix element. The Fermi matrix element for members of the same isospin multiplet can be expressed(Sh74) as

$$\langle\tau\rangle^2 = [\, T(T+1) - T_{Z_i} T_{Z_f} \,]\, \delta_{if}(1-\varepsilon) \quad (2.3)$$

where T is the total isospin and T_{Z_i} is the third projection. The factor $(1-\varepsilon)$ accounts for the reduction in the overlap between the initial and final state nuclear wave function due to isospin mixing. The ratio of the axial to vector β-decay coupling constants, G_a/G_v, is determined experimentally (Wi78) to be 1.251±0.009. The constants C and $(1-\varepsilon)$ are also determined experimentally(Wi78) to be C =

6170(4) and $(1-\varepsilon) = 0.997(3)$. The statistical rate factors f_V, f_A, and f_{EC} are for the vector, axial, and electron capture processes respectively. Given Q_β (Q_β= ME(parent) - ME(daughter)) for a transition f_A and f_V can be estimated using the parameterization of Wilkinson and Macefield(Wi74). In the cases studied in this thesis f_{EC} is small and will be ignored.

Table 2-5 lists the information known about the $^{57}Cu \rightarrow {}^{57}Ni$ β decay. The branching ratios and lifetime are not accurately known. The uncertainty in these quantities will dominate the calculated $\langle \sigma\tau \rangle$ values. Assuming a $3/2^- \rightarrow 3/2^-$ branching ratio of 96(3)% we find $ft = 5.3(4) \times 10^3$ and $\langle \sigma\tau \rangle^2 = 0.10(6)$. The branching for the $3/2^- \rightarrow 1/2^-$ decay was measured to be 3.7±1.7%, and no branching was observed for the $3/2^- \rightarrow 5/2^-$ transition. Based on shell model calculation one would expect ~1% branching to the $5/2^-$, and ~14% to the $1/2^-$, which is not consistent with the experimental values.

Table 2-5: Known properties of ^{57}Cu.

Mass excess = -47.35(5)

Lifetime = 233(16) msec

Branching ratios:

Transition	Branching ratio
$3/2^- \rightarrow 3/2^-$	96(3) %
$3/2^- \rightarrow 1/2^-$	3.7(1.7) %
$3/2^- \rightarrow 5/2^-$	?

2.5.3 Shell Model Predictions

To compare the experimental values with theory we first consider the extreme single particle model. In this model the ^{56}Ni core is assumed to be inert and only one particle in either the 2p3/2, 2p1/2, or 1f5/2 orbits changes isospin projection. With these assumptions it is possible to show(Br77a)

$$\langle\sigma\tau\rangle^2 = 6(2j_f+1)\left\{\begin{matrix} 1/2 & 1/2 & 1 \\ j_f & j_i & l_f \end{matrix}\right\}^2 \delta_{l_i l_f} \qquad (2.4)$$

where $j_f(l_f)$ and $j_i(l_i)$ are the final and initial total angular (orbital) momenta respectively. The results for the transitions considered here are shown in Table 2-5 and are labeled $\langle\sigma\tau\rangle_{sp}$. We find $\langle\sigma\tau\rangle_{sp}/\langle\sigma\tau\rangle_{exp} \approx 3.5$. This result is surprising because one would expect the single particle model to work best for nuclei with one particle outside a closed core, as in the case of ^{57}Cu and ^{57}Ni. To test if the origin of the discrepancy is in the single particle assumption one can compare shell model calculations including core excitations to the single particle value.

Shell model calculations using a given interaction and model space yield a series of wave functions Ψ^{NJT}, where N=A-Core, J is the total spin, and T is the total isospin. These total wavefunctions are constructed of linear combinations of the single particle states ρ^{nlj}, where the superscripts refer only to a single orbit. To perform the

shell model calculation the code OXBASH (Ra84) was used. The model space was the 2p3/2, 2p1/2, and f5/2 orbits and either 0, or 1 holes in the f7/2 core. From the calculated wave functions we extract the density matrix elements for one body operators; $[a^{\dagger}_{j_f} \otimes a_{j_i}]$ ($\sigma\tau$ in this case), coupled to $\Delta J = 1$ and $\Delta T = 1$. The operators $a^{\dagger}_j$ and a_j create and annihilate, respectively, nucleons in the shell model orbit j, where j denotes the single particle state ρ^{nlj}. The density matrix elements are given by

$$D_{j_i j_f} = (2\Delta J + 1)^{-1/2}(2\Delta T + 1)^{-1/2} \times \langle \Psi_f^{NJT} ||| [a^{\dagger}_{j_f} \otimes a_{j_i}]^{\Delta J=1, \Delta T=1} ||| \Psi_i^{NJT} \rangle \qquad (2.5)$$

The density matrix element contains all the shell model information. The total G-T matrix element is determined from

$$\langle \sigma\tau \rangle = [2(2J_i + 1))]^{-1/2} \begin{bmatrix} T_f & 1 & T_i \\ -T_{z_f} & \Delta T_z & T_{z_i} \end{bmatrix} \times \sum_{j_i j_f} D_{j_i j_f} S^{GT}_{j_i j_f} \qquad (2.6)$$

where

$$S^{GT}_{j_i j_f} = \langle \rho_f^{nlj} ||| \underline{\sigma} \cdot \underline{\tau} ||| \rho_i^{nlj} \rangle \qquad (2.7)$$

and the ||| bars represent reduction in both spin and isospin space. The single particle matrix elements, $S^{GT}_{j_i j_f}$,

were calculated with the program DENS (Br84), which also evaluates $\langle\sigma\tau\rangle$ after it reads the one-body transition density matricies output from OXBASH.

2.6 Discussion and Conclusions

The results of the calculations are shown in Table 2-6. The calculations assuming a closed ^{56}Ni core are labeled $\langle\sigma\tau\rangle_{cc}$, and those labeled $\langle\sigma\tau\rangle_{ph}$ assume up to one hole in the ^{56}Ni core. The interaction used in the shell model calculation was taken from VanHees(He81), and reproduces the low-lying excitations in fp shell nuclei. We see that although the shell model calculations give values for the G-T matrix elements which are closer to the measured value, they still are a factor of three high. As mentioned previously Brown and Wildenthal (Br78c,Br83b) have found that to reproduce the measured G-T matrix elements in the sd shell a renormalization factor of 0.6 (0.8 for $\langle\sigma\tau\rangle$ values) must be included in the single particle matrix elements. Even including this factor the discrepancy is large.

Table 2-6: Single particle and shell model $\langle\sigma\tau\rangle$ matrix elements for the $^{57}Cu \rightarrow {}^{57}Ni$, $^{29}P \rightarrow {}^{29}Si$, and $^{55}Ni \rightarrow {}^{55}Co$ β-decays compared with experiment.

Transition	$\langle\sigma\tau\rangle_{sp}$	$\langle\sigma\tau\rangle_{cc}$	$\langle\sigma\tau\rangle_{ph}$	$\langle\sigma\tau\rangle_{exp}$
^{57}Cu with VanHees interaction (He81):				
$3/2^- \rightarrow 3/2^-$	1.291	1.291	0.986	0.32(9)
$3/2^- \rightarrow 1/2^-$	1.155	1.155	0.737	0.25(6)
$3/2^- \rightarrow 5/2^-$	0.0	0.0	0.216	?
^{57}Cu with Mooy interaction (Mo83):				
$3/2^- \rightarrow 3/2^-$	1.291	1.291	0.869	0.32(9)
$3/2^- \rightarrow 1/2^-$	1.155	1.155	0.710	0.25(6)
$3/2^- \rightarrow 5/2^-$	0.0	0.0	0.140	?
^{29}P with Wildenthal interaction (Wi83):				
$1/2^+ \rightarrow 1/2^+$	1.732		0.515	0.440
		full space =	0.575	
^{55}Ni with VanHees interaction (He81):				
$7/2^- \rightarrow 7/2^-$	1.134		0.816	0.508(8)

The discrepancy is probably due to higher order configuration mixing in the ^{56}Ni core. However, this is unexpected because the amount of mixing is inversely proportional to the energy spacing of the levels in first order, and inversely proportional to the n^{th} order of the energy spacing in n^{th} order. Since the correction to the G-T matrix elements was small (see Table 2-6) including 2p-1h states, additional mixing, which would require 3p-2h configurations, should have an even smaller effect. One way to test this conjecture is to study a similar system where a complete shell model calculation is available. The full space calculation can be compared to the 2p-1h calculation to determine in additional mixing can explain the discrepancy. We have done this comparison for the decay of ^{28}P. We find that the 2p-1h calculation gives essentially the same result as the full space calculation. The $\langle\sigma\tau\rangle$ values are only 10% different. The calculated and experimental values for ^{29}P are listed in Table 2-6. We also see that the calculated values for the ^{29}P decay reproduce the 0.8 quenching factor expected. The agreement in the s-d shell indicates the additional quenching in the fp shell may be due to an inadequacy in the interaction of VanHees which was used to calculate the $\langle\sigma\tau\rangle$ values.

To check the interaction we have also included in Table 2-6 the calculated and measured (Ay84) values for the β-decay of ^{55}Ni. Again we see a quenching much stronger than the 0.78 expected, but not as large as the ^{57}Cu

quenching. Finally, as another check of the VanHees interaction, the interaction of Mooy (Mo83) was used to repeat the calculations. As shown in Table 2-6 the results are essentially identical. Since both interactions do a reasonable job in reproducing spectra and electromagnetic transition matrix elements, we would expect them to reproduce the Gamow-Teller matrix elements also. In any event such a large quenching is surprising.

The solution may be that the mechanism of the quenching is a function of A and is stronger in the heavier nuclei, although this is not expected (To83b). Another possibility is that mixing from higher-lying orbits, such as the g9/2 orbit, is contributing. Again considering the energy gap between the 2p3/2 and the g9/2 orbit, this seems very unlikely. It is also possible that the isospin mixing correction is much larger than the $1-\varepsilon = .998$ measured for lighter nuclei (Wi78). If we include the 0.7 renormalization factor, then we find $1-\varepsilon$ must be 0.48(8) to explain the measured ft value. Although one would expect some additional isospin mixing this value seems much too large, considering the largest mixing observed to date gives $1-\varepsilon \approx 0.997$ (Wi78). Presently this large discrepancy remains an interesting and unexplained problem. However due to the lack of an other suitable explanation, the discrepancy seems to be due to an inadequacy in the interaction used in the shell model calculations.

CHAPTER THREE

3.1 Introduction

The nucleus ^{59}Zn is the heaviest $T_z = -1/2$ nucleus for which the mass and lifetime are known (Sh83,Ar84). For this reason its properties are important data for mass predictions (Ke66), studies of Gamow-Teller (G-T) transitions in fp shell nuclei (Ar81,Ar84,Ho81a), and understanding the effects of the Coulomb force in nuclei (Sh83). In particular this nucleus extends the data base for studying the Nolen-Schiffer anomaly (see chapter 4) to the A = 59 mirror pair. With the mass measurement of ^{59}Zn, the A = 59 pair is the heaviest mirror pair with both mass excess known. In this chapter we will review the information previously known on ^{59}Zn, discuss the experimental details of the ^{58}Ni(p,π^-)^{59}Zn reaction used to study ^{59}Zn, and then discuss the implications of the results for mass models and G-T transitions in the fp shell as was done for ^{57}Cu. The implications for the Nolen-Schiffer anomaly will be discussed in chapter 4. When the ^{58}Ni(p,π^-)^{59}Zn reaction was studied an attempt to measure

the $^{40}Ca(p,\pi^-)^{41}Ti$ reaction was also made, and will be discussed at the end of the chapter. We were unable to observe the ^{41}Ti ground state, which has implications on the closed core nature of ^{40}Ca.

The nucleus ^{59}Zn has been observed twice previously. The first observation(Ho81a) was performed at the University of Jyväskylä MC-20 cyclotron. The ^{59}Zn nuclei from the $^{58}Ni(^3He,2n)^{59}Zn$ fusion-evaporation reaction were separated with a He-jet system and the β-decays observed with a Ge(HP) detector. They measured a ^{59}Zn β halflife of 210±20 msec, with the branching ratios shown in Table 3-1. No information was obtained on the mass excess of ^{59}Zn. The second measurement was performed at the University of Tohoku Cyclotron Facility. The ^{59}Zn nuclei were also created via the $^{58}Ni(^3He,2n)^{59}Zn$ reaction but in this case were separated with the Tohoku Isotope Separator On-Line (ISOL)(Fu81). They found a β halflife of 182.0±1.8 msec. The measured branching ratios are also shown in Table 3-1. They were able to extract a ^{59}Zn mass excess by studying the endpoint of the β energy distribution. They deduced a mass excess of -47.23(10) MeV.

3.2 Experimental

As noted in the introduction, Q value measurements of direct reactions usually provide a better technique for measuring the mass and level structure of an unknown nucleus than studying β-decay.